Nonequilibrium Viscous Hypersonic Flows over Ablating Teflon Surfaces

Bilal A. Bhutta,* Dong Joo Song,† and Clark H. Lewis‡
VRA, Inc., Blacksburg, Virginia 24060

Three-dimensional nonequilibrium viscous hypersonic flows over ablating Teflon surfaces are studied using viscous shock-layer and parabolized Navier-Stokes (PNS) schemes. The three-dimensional nonequilibrium PNS scheme developed in this study is inherently stable in the subsonic as well as the supersonic flow regions and, thus, does not require any sublayer approximation. The scheme is formulated in terms of a general curvilinear coordinate system, and a second-order smoothing approach is used to damp the numerical solution oscillations. A new fully implicit and crossflow-coupled shock-fitting approach is used along with a pseudo-unsteady approach to significantly improve the numerical stability and computational efficiency, without compromising solution accuracy. Two test cases for the flow over a sphere-cone vehicle are considered to demonstrate this new three-dimensional nonequilibrium Teflon-air PNS scheme under zero and nonzero angle-of-attack conditions.

Nomenclature

a = local speed of sound
CF, C_f = mass fraction of the Teflon (fuel) species
CI, C_i = mass fraction of ith species
C_p = specific heat at constant pressure
D_{ij} = diffusion coefficient for the ith species with respect to the jth species
$E-$ = electron number density in $1/cm^3$
$KMAX$ = number of grid points in the ξ_3 direction
k = thermal conductivity
Le = Lewis number, $\rho^* \bar{C}_p^* D_{ij}^* / \bar{k}^*$
$LMAX$ = number of grid points in the ξ_2 direction
M = Mach number
m = molecular weight
$\dot{m}$ = nondimensional surface mass-transfer rate, $\dot{m}^*/\rho_\infty^* a_\infty^*$
m_{jk} = $\xi_{2,x_j}\xi_{2,x_k}$
NS = total number of chemical species
n = iteration number
PHI = circumferential angle, ϕ
Pr = Prandtl number
p = static pressure
QW = total wall heat-transfer rate, $Btu/ft^2/s$
R = radial distance from the body axis
RB = local body radius
Re = Reynolds number, $(\rho^* V^* Rn^*)/\mu^*$
RN, Rn = nose radius
T = static temperature
$TINF$ = freestream static temperature, T_∞
u = x component of mass-averaged velocity
u_j = u, v, and w for $j = 1$, 2, and 3
V = total mass-averaged velocity
v = y component of mass-averaged velocity
w = z component of mass-averaged velocity
X = x coordinate measured along the body axis
x_j = x, y, and z for $j = 1$, 2, and 3
ϵ = M_∞/Re_∞
ξ_1 = marching or streamwise coordinate
ξ_2 = coordinate measured from the body to the outer bow shock
ξ_3 = coordinate measured from the windward pitch plane to the leeward pitch plane
γ = ratio of specific heats
ρ = mixture density
μ = mixture viscosity
ϕ = circumferential angle measured from the windward pitch plane
$\dot{\omega}_i$ = production rate of the ith species

Superscripts

j = index in ξ_1 direction
n = index for iteration
$*$ = dimensional quantity
$\bar{}$ = mixture property

Subscripts

i = ith chemical species
j,k,l = indicial notation representing 1, 2, and 3
w = wall quantity
$'$ = partial derivative
∞ = freestream quantity

Introduction

OVER the last several years the prediction of high-altitude (>120 kft) hypersonic re-entry flows has become an area of significant interest and development. At such high altitudes, the characteristic reaction time is much longer than the characteristic flow time, and the vehicle is in the chemical nonequilibrium flow regime for most of the time.

Existing computational fluid dynamics schemes for predicting nonequilibrium hypersonic flows can be broadly classified as 1) boundary-layer (BL) methods, 2) viscous shock-layer (VSL) methods, 3) parabolized Navier-Stokes (PNS) methods, and 4) Navier-Stokes (NS) methods. Hypersonic re-entry flows are, in general, characterized by low Reynolds numbers. Because of such typically low Reynolds number flows, the application of boundary-layer methods has encountered significant difficulties (such as displacement-thickness interaction, streamline tracking, determination of edge conditions,

Presented as Paper 89-0314 at the AIAA 27th Aerospace Sciences Meeting, Reno, NV, Jan. 9-12, 1989; received Feb. 1, 1989; revision received July 1, 1989.

*Chief Scientist. Member AIAA.
†Senior Scientist. Member AIAA.
‡President. Associate Fellow AIAA.

etc.). The nonequilibrium laminar boundary-layer analysis method of Blottner et al.[1] is a particular example of such solution methods. As far as nonequilibrium Navier-Stokes methods are concerned, there are very few (if any) practical schemes available to date. Even so, such methods are typically very time consuming and not well suited for any practical design and analysis study. The VSL and PNS methods, on the other hand, have shown great potential for analyzing such nonequilbrium viscous reentry flows. Studies of Swaminathan et al.,[2] Kim et al.,[3] and Song and Lewis[4] have shown that the VSL scheme provides a very effective tool for accurately and efficiently predicting the flowfield in regions where the flow is attached in the crossflow direction. While the VSL schemes cannot be used in regions of crossflow separation, the PNS schemes do not suffer from such a limitation. Thus, the nonequilibrium PNS schemes provide an accurate and efficient method for treating three-dimensional nonequilibrium hypersonic flows. Even under large angle-of-attack conditions the flowfield in the nose region remains attached in the crossflow direction. Consequently, the VSL schemes can still be used to provide the necessary starting solution to initiate the afterbody PNS solution scheme.

The temperatures encountered during re-entry are typically very high and cause a significant amount of dissociation and ionization of the air molecules within the shock layer. These shock-layer properties directly influence the gas chemistry in the wake. Furthermore, such re-entry flows are typically associated with large surface heating rates, which, in turn, cause substantial surface ablation. If the ablation products are in significant amounts, the gas chemistry in the shock layer can also be affected. Especially because of the different specific heats of the ablation products and their subsequent reactions with the surrounding gas species, the shock-layer temperature distribution can be quite different. Song and Lewis[4] studied the effects of carbon ablation using a nonequilibrium VSL scheme and observed that surface ablation caused a significant reduction in the peak shock-layer temperature. They also found that carbon ablation products increased the stagnation point wall heat-transfer rates. The existing theoretical methods for predicting nonequilibrium Teflon-air flows are very limited, and, more importantly, use a boundary-layer approach to predict the viscous flowfield.[5-7] Such a boundary-layer approach may not be valid under the low-Reynolds-number and high-Mach-number conditions typical of such nonequilibrium re-entry flowfields.

In this study we have developed a new three-dimensional, nonequilibrium PNS scheme for accurately predicting the effects of Teflon ablation into air under hypersonic flight conditions. The scheme uses a general curvilinear coordinate system. This PNS scheme is also unconditionally time-like in character in the marching direction and, thus, does not require any sublayer approximation. A new fully implicit shock-fitting scheme has been developed. This new shock-fitting scheme is coupled in the crossflow direction and subtantially enhances the stability of the solution scheme. A pseudounsteady approach is used to provide numerical efficiency without having to sacrifice solution accuracy.

Two test cases have been considered to demonstrate this new three-dimensional nonequilibrium PNS capability for studying the effects of Teflon ablation into air. These test cases are for 0 and 1 deg angle-of-attack flow over a 7-deg sphere-cone vehicle at an altitude of 175 kft and a Mach number of 20. Both of these test cases involve Teflon ablation at the surface. The results of these test cases demonstrate the accuracy and efficiency characteristics of the three-dimensional nonequilibrium PNS scheme developed.

Chemical Modeling of Teflon and Air Mixture

The oxidation and reduction chemistry of Teflon (C_2F_4) is not fully understood. Teflon is a fluorocarbon polymer compound, and the possible species from the oxidation, reduction, and ionization of a system composed of F, C, N, and O can be numerous.[8] Some of these species can be identified as trace, while the reaction mechanisms of some species are not even well understood.

Description of the Chemical Model

To develop a chemical model to define the Teflon-air chemical system, we started with a system composed of 32 species. The species considered were O, O_2, N, N_2, NO, C, CO, CO_2, Na, F, F_2, CF_2, CF_4, COF_2, C_2F_4, NO^+, O^-, O_2^-, Na^+, F^-, e^-, C_2F_2, CF_3, CF, FO, FCN, F_2O, FCO, FO_2, FNO, $C_2F_4^+$, and CF_3^+. Some of the important previous research taken into consideration before deciding upon this chemical system included the works of Blottner et al.,[1] Song and Lewis,[4] Braun,[5] Cresswell et al.,[6] Langan et al.,[9] and Appleton et al.[10] In this chemical model, Na and Na^+ have been included to simulate the effects of sodium contamination in the ablation products. The ionization potential of Na^+ is less than NO^+; consequently the ionization of Na will contribute substantially to the electron concentration in the shock layer. In our study, we introduced small amounts of sodium (133 ppm) at the wall to simulate this sodium contamination. This approach is similar to the one used by Cresswell et al.[6]

Out of these original 32 species we were able to neglect the last 11 species; namely, C_2F_2, CF_3, CF, FO, FCN, F_2O, FCO, FO_2, FNO, $C_2F_4^+$, and CF_3^+. The first nine of these species were neglected because their concentrations under various conditions were typically far less than 0.5×10^{-5} and, also, their reaction mechanisms were not clearly understood. The ionized species $C_2F_4^+$ and CF_3^+ were neglected because their ionization potentials are much higher than the ionization potential of NO^+. Furthermore, the ionization reactions of C_2F_4 and CF_3 are not clearly understood to date.

With these assumptions we finally decided upon a 21-species (O, O_2, N, N_2, NO, C, CO, CO_2, Na, F, F_2, CF_2, CF_4, COF_2, C_2F_4, NO^+, O^-, O_2^-, Na^+, F^-, and e^-) Teflon-air system described by 28 gas-phase reactions. The first seven of these reactions are based on the seven-species nonequilibrium-air work of Blottner et al.[1] and Miner and Lewis.[11] Reaction 8 is the NO dissociation reaction and was introduced based on the studies of Cresswell et al.[6] Reactions 9–11 are based on the studies of Langan et al.[9] and Appleton et al.[10] and involve the dissociation and recombination of CO and CO_2. These CO and CO_2 reactions were also used by Song and Lewis[4] for their studies of carbon ablation into nonequilibrium air. The last 17 reactions (reactions 12–28) are based on the work of Braun[5] and Cresswell et al.,[6] and involve the reactions of Na, F, F_2 and other fluorocarbon species.

Reaction-Rate Data

The reaction-rate data for the 28-reaction system were gathered from several sources. The rate data for reactions 1–7 are based on the data of Bortner,[12] and the rate data for reaction 8 are based on the rate data used by Cresswell et al.[6] The rate data for reaction 9 are based on the recommendations of Langan et al.[9] The forward reaction-rate data for reactions 10 and 11 are based on the work of Appleton et al.,[10] and the backward reaction rates are calculated using the equilibrium constants of Schofield.[13] The data rate for reactions 12–28 are based on the works of Braun,[5] Cresswell et al.,[6] and Modica and LaGraff.[14,15]

Thermodynamic and Transport Property Data

The thermodynamic data for N_2, O_2, N, O, NO, NO^+, and CO were obtained from Browne[16-18] for the temperature range of 100–60,000 K. The C and CO_2 data were obtained from Esch et al.[19] and Gordon and McBride.[20] However, due to the lack of thermodynamic properties of CO_2 above 10,000 K, the specific heat of CO_2 above 10,000 K was assumed constant and the enthalpy data was consistently calculated. The data for NA and Na^+ were obtained from Gordon and McBride[20]

for 300-5000 K, and from Browne and Miller[8] for 5000-15,000 K. For the 15,000-60,000 K temperature regime, the specific heats for Na and Na^+ were assumed as constant and enthalpies were calculated by integrating this specific heat data. The thermodynamic data of O^- were obtained from Gordon and McBride[20] for the temperature range of 100-6000 K. From 6000 to 60,000 K these data were extended by assuming a constant specific heat and by integrating this specific heat data to obtain the enthalpy data. The data for the remaining ablation products (O_2^-, CF_2, CF_4, F, F_2, F^-, C_2F_4, and COF_2) were obtained from Browne[21] and Browne and Miller[8] for the temperature range of 100-15,000 K. From 15,000 to 60,000 K these data were extrapolated by assuming constant specific heat for the species.

The viscosity data for the N_2, O_2, N, O, NO, and NO^+ species for 100 to 15,000 K were obtained from the data of Blottner et al.,[1] which are actually based on the data of Yos.[22] The viscosity data of C, CO, and CO_2 were obtained from Moss.[23,24] The viscosity data for Na, CF_2, CF_4, F, F_2, and C_2F_4 were obtained from the data of Svehla[25] for temperatures from 300 to 5000 K. For the high temperature range above 5000 K, the viscosities were determined using the Neufeld formula[26] and were based on appropriate values for the collision cross sections and reduced temperatures. For Na, CF_2, CF_4, F, and F_2 the collision cross sections and reduced-temperature data of Svehla[25] were used, while for C_2F_4 these data were obtained from Reid et al.[27] For Na^+, F^-, O_2^-, O^-, and COF_2 the viscosity data were obtained from Biolsi[28] for temperatures up to 15,000 K.

Mathematical and Numerical Formulation

The coordinate system used for the present three-dimensional PNS scheme is a general curvilinear coordinate system (ξ_1,ξ_2,ξ_3) shown in Fig. 1. The origin of the coordinate system is at the tip of the blunt nose, and the x axis is aligned with the axis of the body. The ξ_1 coordinate is along the body and is also the marching direction. The ξ_2 coordinate stretches from the body to the outer bow shock and lies in an axis-normal plane. The ξ_3 coordinate is measured in the crossflow direction from the windward pitch plane. In general, it is assumed that the (x,y,z) space is uniquely transformable to the (ξ_1,ξ_2,ξ_3) space through relations of the form

$$\xi_j = \xi_j(x,y,z) \tag{1}$$

The transformation given by Eq. (1) is generally difficult to obtain; however, the metric derivatives for the inverse transform can be easily obtained numerically. At each grid point, this information about the inverse-transformation metrics is used to determine the transformation Jacobians and the metric derivatives (ξ_{j,x_i}) for the transformation given by Eq. (1).

Governing Equations

The full Navier-Stokes equations[29] governing the three-dimensional nonequilibrium flow problem can be written in a nondimensional form as

$$(\boldsymbol{e}_j - \epsilon \boldsymbol{g}_j)_{,x_j} = \boldsymbol{p} \tag{2}$$

We choose our unknowns to be density ρ, density-velocity products ρu, ρv, and ρw, the density-temperature product ρT, and the pressure p. Thus, our vector of unknowns is

$$\boldsymbol{q} = [\rho, \rho u, \rho v, \rho w, \rho T, p]^T \tag{3}$$

Following the approach of Peyret and Viviand,[30] it can be shown that Eq. (2) can be transformed into the general curvilinear coordinate system (ξ_j); i.e.,

$$(\boldsymbol{f}_j - \epsilon \boldsymbol{s}_j)_{,\xi_j} = \boldsymbol{h} \tag{4}$$

Equation (4) is elliptic in the ξ_1, ξ_2, and ξ_3 directions. If we neglect the diffusion and dissipation effects in the ξ_1 and ξ_3 directions and assume a constant Lewis number, we can combine Eqs. (4) and (2) in the following vectorial equation

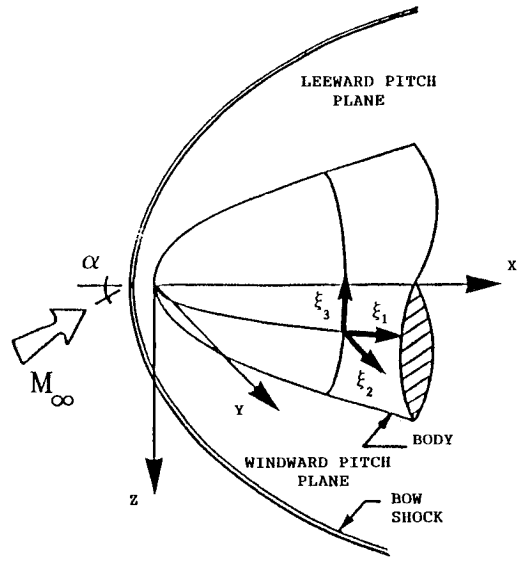

Fig. 1 General curvilinear coordinate system.

$$\boldsymbol{f}_{j,\xi_j} - \epsilon \boldsymbol{s}_{,\xi_2} = \boldsymbol{h} \tag{5}$$

These five equations representing the differential conservation of mass, momentum, and energy are mathematically closed by using the equation of state for the particular gas model being used. In the case of a finite-rate chemically reacting Teflon-air mixture, the gas is assumed to be a mixture of perfect gases. The equation of state for such a reacting gas mixture is given by

$$p - \rho T/\bar{m} = 0 \tag{6}$$

where $\bar{m}$ is the nondimensional mixture molecular weight defined as $\bar{m} = \bar{m}^*/\bar{m}^*_\infty \gamma_\infty$.

The mixture thermodynamic properties (such as $\bar{m}$, $\bar{k}$, $\bar{C}_p$, $\bar{\mu}$, Pr) require a knowledge of the species concentrations C_i that are obtained from the three-dimensional species conservation equations.[29] These equations are transformed into the (ξ_1,ξ_2,ξ_3) coordinate system, and the resulting equations are parabolized by neglecting diffusion effects in the ξ_1 and ξ_3 directions. The final thin-layer parabolized species conservation equations are written in a nonconservative form as

$$\rho u_k \xi_{j,x_k} C_{i,\xi_j} + \epsilon\, [\xi_{2,x_j}\, Le\, (\bar{\mu}\xi_{2,x_j}/Pr)_{,\xi_2}]\, C_{i,\xi_2} + \epsilon\, [\bar{\mu} m_{kk}\, Le/Pr]\, C_{i,\xi_2\xi_2} = \dot{\omega}_i \tag{7}$$

where $i = 1,2,\ldots,(NS-1)$.

The system of equations represented by Eqs. (5) and (7) is closed through a knowledge of the thermodynamic and transport properties of the mixture; namely, $\bar{C}_p$, $\bar{k}$, $\bar{m}$, $\bar{\mu}$, Pr, and Le.

Local Linearizations and Numerical Formulation

The overall nonequilibrium PNS problem represented by Eqs. (6) and (10) is well posed. However, the number of unknowns involved is very large (i.e., ρ, ρu, ρv, ρw, ρT, p, $\bar{C}_p$, $\bar{k}$, $\bar{m}$, $\bar{\mu}$, Pr, C_1, C_2,..., C_{NS}). A simultaneous solution of these quantities would be beyond the practical limits of present computational facilities, even perhaps future supercomputers. Even so, the solution of a practical problem would be very expensive and time consuming. However, for many practical problems, the coupling between the fluid mechanics (ρ,

ρv, ρw, ρT, and p) and the chemistry ($\bar{C}_p$, $\bar{m}$, $\bar{k}$, $\bar{\mu}$, Pr, C_1, C_2,..., C_{NS}) is not very strong. With this idea in mind, we can decouple the overall nonequilibrium PNS problem into a fluid mechanics problem and a chemistry problem.

The fluid mechanic problem is represented by Eq. (5), where the chemistry is assumed as known. The chemistry problem involves the solution of Eq. (7) and the determination of the transport properties of the mixture, where the solution to the fluid mechanics is assumed as known. The coupling between the fluid mechanics and the chemistry is treated in an iterative manner. Thus, for each iteration at a given marching step we first solve the fluid mechanics problem, and then we solve the chemistry problem based on the solution to the fluid mechanics problem. With this updated chemistry, the fluid mechanics problem is solved once again, and the cycle is repeated until acceptable convergence is achieved. In this manner, in the limit of convergence, we have a fully iterated solution that completely accounts for the coupling between the fluid mechanics and the chemistry of the flowfield.

Solution of the Fluid Mechanics Problem

Let us denote the iteration level by the index n, so that the iteration at which we seek the the solution is represented by the superscript $n+1$, and the previous iteration (the solution to which is known) is represented by the superscript n. Thus, for the $n+1$ iteration at the $j+1$ marching step we can write Eq. (5) as

$$\boldsymbol{f}^{j+1,n+1}_{k,\xi_k} - \epsilon \boldsymbol{s}^{j+1,n+1}_{,\xi_2} = \boldsymbol{h}^{j+1,n+1} \tag{8}$$

If we assume that the solution at the $n+1$ iteration is close to the solution at the nth iteration, we can use a first-order Taylor series expansion around the previous iteration. Thus, we see that by expanding the solution around the nth iteration and using two-point streamwise differencing, we can write Eq. (8) as

$$(\boldsymbol{A}_1/\Delta\xi_1 - \boldsymbol{A}_0)^n \cdot \Delta\boldsymbol{q}^{n+1} + [(\boldsymbol{A}_2 - \epsilon \boldsymbol{M})^n \cdot \Delta\boldsymbol{q}^{n+1}]_{,\xi_2} + (\boldsymbol{A}_3^n \cdot \Delta\boldsymbol{q}^{n+1})_{,\xi_3} = -[\boldsymbol{f}_{k,\xi_k} - \epsilon \boldsymbol{s}_{,\xi_2} - \boldsymbol{h}]^{j+1,n} = \boldsymbol{g}^{j+1,n} \tag{9}$$

Equation (8) is elliptic in the ξ_2 and ξ_3 directions so that for second-order accuracy we use central-difference approximations for all ξ_2 and ξ_3 derivatives. However, the use of central-differenced schemes is typically associated with solution oscillations.[31-38] To damp these solution oscillations, it is necessary to add some additional higher-order diffusion terms to Eq. (8). It can be shown that by extending the basic approach of Bhutta et al.[31] and Bhutta and Lewis[32-35] to second-order accuracy, we can rewrite Eq. (8) in terms of an intermediate solution χ^{j+1} as

$$[\boldsymbol{f}_k(\chi^{j+1})]_{,\xi_k} = \epsilon\,[\boldsymbol{s}(\chi^{j+1})]_{,\xi_2} + \boldsymbol{h}(\chi^{j+1}) + \mathcal{O}(\Delta\xi_2)^2 + \mathcal{O}(\Delta\xi_3)^2 \tag{10}$$

The actual solution that we seek at the $j+1$ step is related to this intermediate solution by

$$(\chi_1)^{j+1} = \chi^{j+1} + \chi_{,\xi_3\xi_3}\Delta\xi_3^2/4 \tag{11a}$$

$$\boldsymbol{q}^{j+1} = (\chi_1)^{j+1} + (\chi_1)_{,\xi_2\xi_2}\Delta\xi_2^2/4 \tag{11b}$$

Solution of the Chemistry Problem

Using the solution of the fluid mechanics problem [Eqs. (10) and (11)], the transport properties of the 21-species Teflon-air system can now be determined. This information is then used to evaluate the production rates ($\dot{\omega}_i$) for the various species involved. In treating the species conservation equations in such a decoupled manner, it is necessary to split the overall production term into two parts[1,11] as follows:

$$(\dot{\omega}_i/\rho) = \dot{\omega}_i^0 - \dot{\omega}_i^1 C_i \tag{12}$$

This separation balances the explicit and implicit sides of the species conservation equations and results in a stable solution. Both of these components of the species production term are functions of the species concentrations, local density, and local temperature. In our study we took a new approach of partially linearizing the production terms, where the production terms are still separated into left-hand side and a right-hand side contributions. These components are then linearized based on the flowfield and chemistry information from the previous marching step. Since this linearization is only partial and is done on quantities that indeed change very slowly (especially in the PNS afterbody region), the errors introduced are very small. However, the computing time efficiency achieved is substantial.

With the species production terms written as in Eq. (12), we can write the parabolized species conservation equations [Eq. (7)] as

$$a_0^n C^{n+1}_{i,\xi_1} + a_1^n C^{n+1}_{i,\xi_2} + a_2^n C^{n+1}_{i,\xi_2\xi_2} + a_3^n C_i^{n+1} + a_4^n C^{n+1}_{i,\xi_3} = a_5^n \tag{13}$$

where the coefficients a_0, a_1, a_2, a_3, a_4, and a_5 are functions of the flowfield variables, the transport properties of the gas mixture, and the species production terms. The solution of Eq. (13) is obtained by using a two-point backward-difference formula for the ξ_1 derivative and central-differenced approximations for the ξ_2 and ξ_3 derivatives.

Pseudounsteady Solution Algorithm

Using a two-point streamwise differencing and central-differenced approximations in the ξ_2 and ξ_3 directions, the final differenced equations corresponding to the fluid mechanics problem are written in the block-pentadiagonal form as given in Eq. (9). It should be noted that the right-hand side of Eq. (9) consists of the governing differential equations corresponding to the fluid mechanics problem written at the nth iteration level, and it goes to zero in the limit of convergence. As discussed by Bhutta and Lewis,[32-35] under these conditions the exact form of the left-hand implicit terms is of no great consequence except that it affects the convergence path of the solution. With this idea in mind we do not update the Jacobian matrices beyond the first iteration. In this study, this pseudounsteady approach is extended to three dimensions by assuming that crossflow derivatives can be linearized from the previous iteration. With this assumption the convective crossflow derivatives appear only in the explicit right-hand side vector. A somewhat similar approach was used by Helliwell et al.[39] and Agarwal and Rakich.[40,41] By doing so we obtain the final differenced equations as

$$(\boldsymbol{A}_1/\Delta\xi_1 - \boldsymbol{A}_0)^{n=1} \cdot \Delta\chi^{n+1} + [(\boldsymbol{A}_2 - \epsilon \boldsymbol{M})^{n=1} \cdot \Delta\chi^{n+1}]_{,\xi_2} = -[\boldsymbol{f}_{k,\xi_k} - \epsilon \boldsymbol{s}_{,\xi_2} - \boldsymbol{h}]^{j+1,n} = \boldsymbol{g}^{j+1,n} \tag{14}$$

The converged limit of Eq. (14) is the same as the converged limit of Eq. (9). However, Eq. (14) represents a block-tridiagonal set of equations rather than the block-pentadiagonal system represented by Eq. (9) and is considerably more efficient and faster to solve.

A similar approach is also used to simplify the species conservation equations. In the case of the species conservation equations, the convective crossflow derivatives of the species concentrations (C_{i,ξ_3}) were estimated from the previous iteration and included in the explicit right-hand side term as

$$a_0^n C^{n+1}_{i,\xi_1} + a_1^n C^{n+1}_{i,\xi_2} + a_2^n C^{n+1}_{i,\xi_2\xi_2} + a_3^n C_i^{n+1} = (a_5 - a_4 C_{i,\xi_3})^n \tag{15}$$

In this way the species conservation equations can be solved using a simple tridiagonal solver, rather than a pentadiagonal solver.

It should be mentioned that in 1987, for his Master's thesis, Pluntze[42] attempted an independent study to replicate our baseline perfect-gas PNS scheme. The work was supervised by Prof. J. R. Baron; however, the approach followed lacked some important features that led Pluntze[42] to certain incorrect conclusions. Unfortunately, we were only informed of the study after it had been completed; nevertheless, we still reviewed the material involved and indicated in writing[43] the various deficiencies in the approach taken. Some of the major deficiencies were 1) a lack of adequate crosschecking because, for some reason, Pluntze used a two-dimensional approach instead of an axisymmetric approach, which could have been checked against a number of our published results; 2) the step-size studies incorrectly emphasized starting from an inaccurate set of initial conditions without any emphasis on the numerical solution accuracy; 3) a sustained accumulation of numerical errors (an accuracy problem) was incorrectly confused with solution departure (a mathematical invariant); and 4) the eigenvalue analysis was inappropriately done on the finite-differenced form of the equations rather than the governing equations. The latter is inappropriate because such an analysis of the finite-differenced equations may lead to numerical restrictions that are a reflection of the numerical scheme used and are not necessarily reflective of the character of the governing equations. For example, the classical CFL condition is only a numerical restriction for the unconditionally time-like (in this case hyperbolic) wave equation.

Boundary Conditions

The problem represented by the governing PNS equations is a split-boundary-value problem; that is, the equations are hyperbolic-parabolic in the ξ_1 direction and elliptic in the ξ_2 and ξ_3 directions. Thus, to solve the problem completely, we need initial conditions to be specified at the start of the marching procedure, boundary conditions to be specified at the wall and at the outer bow shock, and boundary conditions to be specified in the windward and leeward pitch planes (for flows with a pitch-plane of symmetry).

Initial Conditions

The initial conditions to start the nonequilibrium PNS solutions were obtained from a VSL blunt-body solution scheme using the same nonequilibrium Teflon-air system. The quality of such VSL solutions has been discussed in great detail by Bhutta et al.,[31] Bhutta and Lewis,[32-35] Thompson et al.,[44] and Swaminathan et al.[2] The VSL blunt-body solution is interpolated to obtain the starting solution at the initial data plane (IDP) for the three-dimensional PNS afterbody solution. We typically generate the IDP at the most upstream nose-afterbody tangent point location.

Wall Boundary Conditions

For the fluid mechanics problem of the nonequilibrium PNS equations, the boundary conditions at the wall consist of six independent relations representing the nature of the gas mixture and the physical conditions at the wall; i.e., 1) the equation of state of the gas $[f(\rho,p,T,C_i) = 0]$, 2) no-slip boundary condition for $u[\rho u = 0]$, 3) boundary condition for $v[\rho v = (\rho v)_w]$, 4) boundary condition for $w[\rho w = (\rho w)_w]$, 5) a specified wall temperature $[(\rho T) = \rho T_w]$, and 6) zero pressure derivative in the ξ_2 direction $[p_{,\xi_2} = 0]$. The first five boundary conditions are easy to visualize as they represent the actual physical conditions at the wall. The sixth boundary condition on the pressure derivative comes from a boundary-layer-type analysis performed at the wall. The preceding set of boundary conditions is well posed and forms a linearly independent set.

In modeling blowing conditions at the wall, it is assumed that the surface blowing is in an axis-normal plane. This is necessary to avoid negative axial velocities at the wall, which mathematically violates the parabolic flow assumption. In terms of nondimensionalized variables we have

$$(\rho v)_w = \dot{m} \sin\phi \tag{16a}$$

$$(\rho w)_w = \dot{m} \cos\phi \tag{16b}$$

For the chemistry problem [Eq. (15)], we assume that the body surface is an equilibrium-catalytic wall $[C_i = C_i(p_w, T_w, \dot{m})]$. Even with this equilibrium-wall assumption, the species composition at the wall is a complicated problem to treat. In our approach, however, we assume that the species boundary conditions at the wall can be obtained by solving the species conservation equations for a nonreacting binary mixture composed of Teflon and air species. Similar ideas have also been used by Baron[45] in his earlier work. In this approach, we assume that the fuel species (C_f) are transported away from the wall by convection and also carried away from the wall due to diffusion. In the remaining shock layer the concentration of fuel species is determined from the parabolized conservation equation for C_f. The boundary condition at the bow shock corresponds to $C_f = 0$, which is consistent with the frozen shock-crossing approximation used for the overall solution.

Boundary Conditions at the Shock

The boundary conditions at the outer bow shock are, however, much more involved. These boundary conditions involve a fully implicit and crossflow-coupled shock-fitting approach, and the bow shock location is predicted as a part of the marching solution.

Circumferential Boundary Conditions

The three-dimensional nonequilibrium PNS developed can only treat flows with a pitch plane of symmetry; that is, the vehicle geometry is symmetric with respect to the pitch plane, and there is no yaw. For such a case, the boundary conditions in the windward and leeward pitch planes consist of reflective or symmetric boundary conditions. The symmetric and reflective boundary conditions used in the present study are based on the second-order crossflow boundary conditions used by Kaul and Chaussee[37] and Shanks et al.[38]

Fully Implicit Shock-Fitting Procedure

In this study we have developed a new fully implicit and crossflow-coupled shock-fitting scheme. In this scheme the bow shock location is iteratively predicted as the solution marches down the body and various gas models (perfect-gas, equilibrium-air, and nonequilibrium-air) can be accurately treated in a unified manner. The important features of this bow shock-fitting approach are as follows:

1) Unlike earlier noniterative shock-propagation approaches,[37,38,46] the present approach does not assume the flowfield behind the shock to be inviscid. This can be quite important when strong flowfield gradients exist behind the shock, as may be the case in the nose-dominated region and in regions where the bow shock starts to interact with the embedded shock waves (or compression waves) originating from the body.

2) Unlike the iterative shock-fitting approaches of Helliwell et al.[39] and Lubard and Helliwell,[47] the present shock fitting approach is not only for a general curvilinear coordinate system but also does not increase the matrix size of the block-matrix solution between the body and the shock.

3) Unlike any earlier iterative or noniterative bow shock-fitting scheme, the present shock-fitting scheme does not neglect the crossflow-coupling effects at the shock. This results in accurate and smooth shock shapes even when there are strong crossflow variations of the conditions behind the shock. This can be especially important when dealing with complex three-dimensional configurations where the three-dimensional na-

ture of the body can interact with the bow shock and substantially distort it. Similar strong crossflow variations may also occur on simple configurations when pitched at large angles of attack.

In developing the present bow-shock-fitting scheme, we assume that from one iteration to the next the shock points move along the ξ_2 grid line. This direction corresponds to the intersection of the ξ_1 = const and ξ_3 = const surfaces. This assumption allows us to reduce the size of unknowns to be solved. The final solution has only one additional unknown at the shock, which completely defines the spatial movement of the shock point. This smaller size of the unknowns is very important for a faster iterative solution and faster convergence characteristics of the overall implicit shock-prediction scheme. Furthermore, this simplification only represents a certain constraint on the direction in which the shock point moves and does not affect the accuracy of the shock-crossing solutions.

If we denote the amount of shock motion in the ξ_2 direction by Δ_s, it can be shown that the various metric derivatives and the shock-normal and shock-tangent velocity components can be expressed in terms of this shock motion and the flowfield conditions behind the shock surface. Having defined the relevant velocity components for the purpose of writing the five Rankine-Hugoniot frozen shock-crossing equations (representing the conservation of mass, momentum, and energy), we note that we have actually seven unknowns at the shock, which can be written in a vectorial form as

$$q_s = [\rho, \rho u, \rho v, \rho w, \rho T, p, \Delta]_s^T \tag{17}$$

Thus, we need two more equations to close the system of equations at the shock. One of these additional equations is the equation of state of the gas, and the other equation is provided by applying the differential continuity of mass equation behind the shock. As we see, no approximation other than the assumption of a frozen Rankine-Hugoniot shock has been made. These equations are equally valid whether the conditions behind the shock are viscous- or inviscid-dominated or whether substantial flowfield gradients exist behind the shock. These equations can now be linearized around the pervious iteration. Using central-differenced approximations for ξ_3 derivatives and backward-differenced approximations for ξ_1 and ξ_2 derivatives, we can rewrite these equations in the form

$$(A_s)_k^n \cdot (\Delta q_s)_{k-1}^{n+1} + (B_s^*)_k^n \cdot (\Delta q_s)_k^{n+1} + (C_s)_k^n \cdot (\Delta q_s)_{k+1}^{n+1} + \begin{bmatrix} (D_s)_k^n & 0 \\ 0 & 0 \end{bmatrix} \cdot \begin{bmatrix} \Delta\chi_{k,LMAX}^{n+1} - 1 \\ 0 \end{bmatrix} = (g_s^*)_k^n \tag{18}$$

As can be seen from Eq. (18), the solution of the equation at the shock is coupled to the inner flowfield solution through $\Delta\chi_{k,LMAX-1}^{n+1}$. To finally solve this system of equations, we note that Eq. (14) shows that the inner flowfield solution (from $\ell = 1, 2, \ldots, LMAX - 1$) is decoupled in the crossflow direction. Thus, a forward substitution approach can be used for all crossflow planes to develop recursive relations relating the solution vectors in the ξ_2 direction. Using this approach, the inner flowfield solution can be related to the shock-point solution vector Δq_s^{n+1} through relations of the form

$$\Delta\chi_{k,LMAX-1}^{n+1} = -[R_{k,LMAX-1} \quad 0] \cdot (\Delta q_s)_k^{n+1} + r_{k,LMAX-1}^n \tag{19}$$

After substituting Eq. (19) into Eq. (18), we can reduce Eq. (18) to the form

$$A_k^n \cdot (\Delta q_s)_{k-1}^{n+1} + B_k^n \cdot (\Delta q_s)_k^{n+1} + C_k^n \cdot (\Delta q_s)_{k+1}^{n+1} = g_k^n \tag{20}$$

Equation (20) is now solved using appropriate reflective and symmetric boundary conditions in the leeward and windward pitch planes of symmetry. This solution gives simultaneously the Δq_s^{n+1} vectors at each shock point ($k = 1,2,\ldots, KMAX$). Using the shock-point solution, we can obtain the intermediate solution vector $\Delta\chi^{n+1}$ for all interior points. The final smoothed solution at these interior points is then determined from Eqs. (11a) and (11b).

Results and Discussion

To demonstrate the accuracy and efficiency of the proposed three-dimensional PNS scheme, we studied two test cases.[48] Cases 1 and 2 are for the flow around a sphere-cone vehicle at an altitude of 175 kft and a Mach number of 20.7. The vehicle geometry consists of a 7-deg sphere cone with a 2-in. nose radius. Case 1 is for 0 angle-of-attack conditions, whereas case 2 is for 1 deg angle-of-attack conditions. Both of these cases assume Teflon ablation at the wall; however, the mass-transfer distributions used for these cases are different.

Case 1 Calculations

Apart from the calculations using the present nonequilibrium PNS scheme, we also studied this case with a Teflon-air VSL scheme. This Teflon-air VSL scheme was also used to generate the IDP for starting the present PNS afterbody calcu-

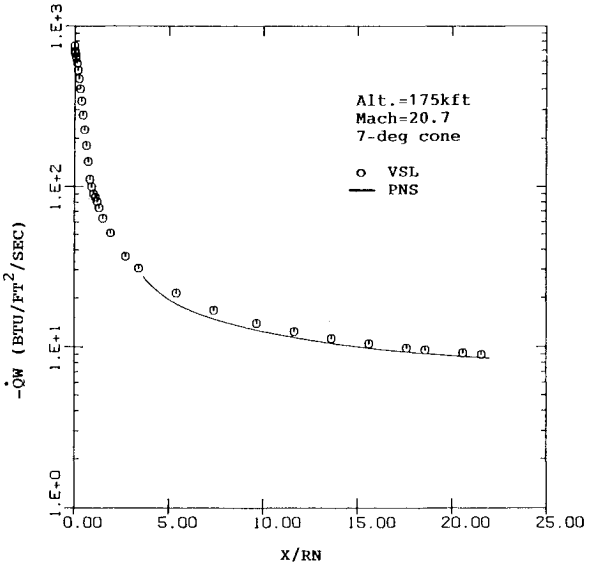

Fig. 2 Axial distribution of wall heat-transfer rates for case 1.

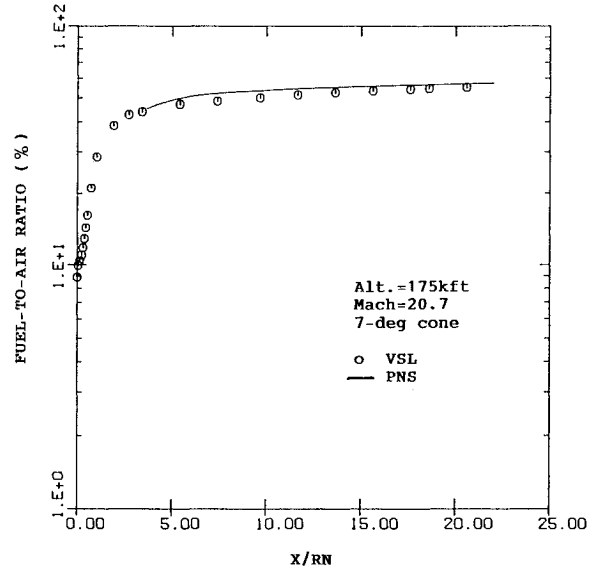

Fig. 3 Axial distribution of fuel-to-air ratios for case 1.

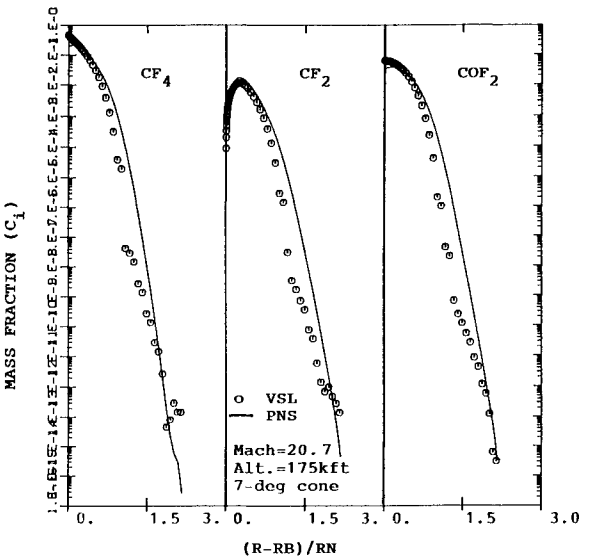

Fig. 4 CF_4, CF_2, and COF_2 concentration profiles at $x/Rn = 22$ for case 1.

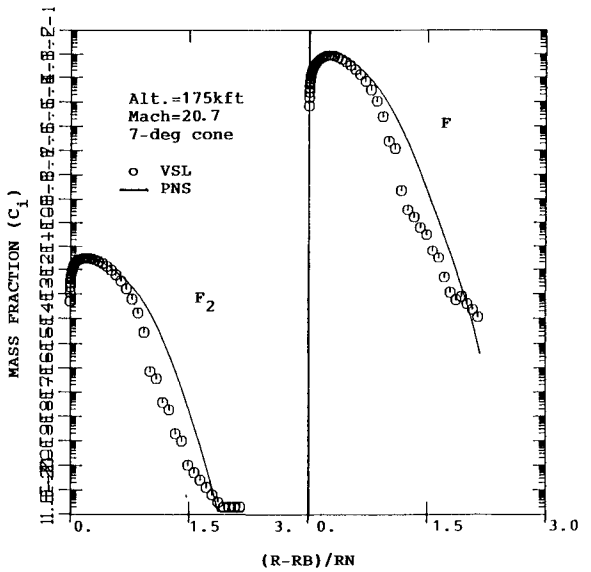

Fig. 5 F and F_2 concentration profiles at $x/Rn = 22$ for case 1.

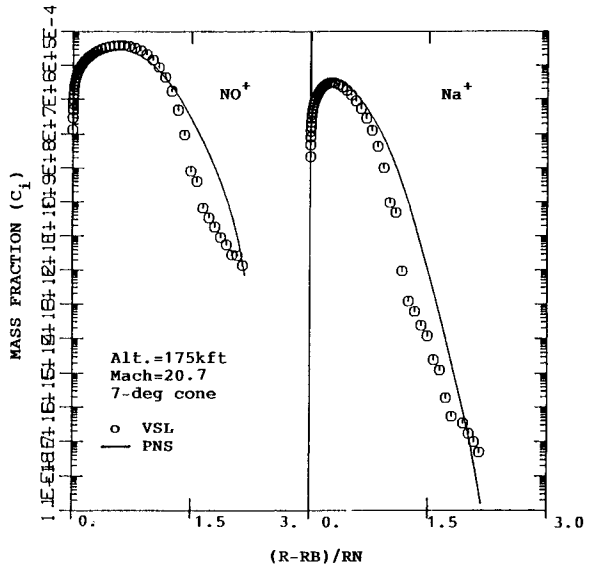

Fig. 6 NO^+ and Na^+ concentration profiles at $x/Rn = 22$ for case 1.

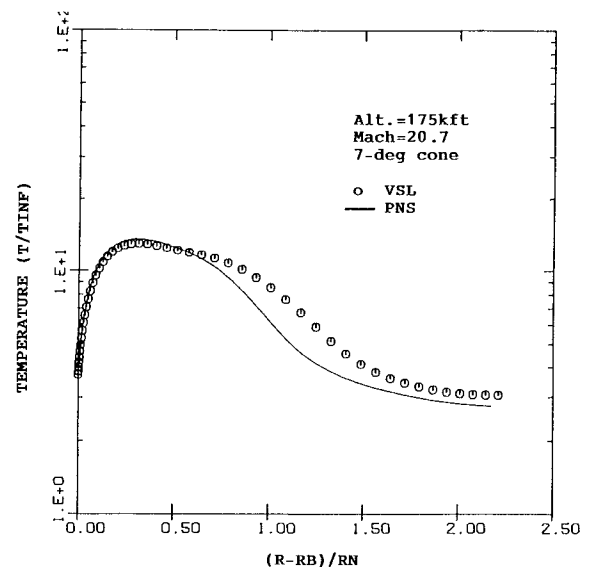

Fig. 7 Temperature profiles at $x/Rn = 22$ for case 1.

lations. This axisymmetric PNS solution uses one circumferential plane and 50 points between the body and the shock. The grid spacing at the wall for this case was 0.01% of the local shock-standoff distance.

Comparison of Surface-Measurable Quantities

Figure 2 shows a comparison of the wall heat-transfer rates and shows excellent agreement between the globally iterated VSL and the corresponding PNS predictions. In this case, the diffusion heat-transfer contribution is about twice as much as the corresponding conduction component. The results show that both diffusion and conduction components are in almost perfect agreement, which is exceptionally good considering the fact that the VSL and PNS equations (as well as the solution schemes) are quite different. Clearly, this is due to the accuracy of our fluid-mechanics and chemistry solutions. Although not shown here, the VSL and PNS predictions of wall pressure and skin friction are in excellent agreement and, consequently, there is practically no difference in the axial-force coefficient predicted by the two schemes.

Comparison of Species Concentrations

Figure 3 shows the comparison between the VSL and PNS predictions of the fuel-to-air ratio at the wall. The results show that the differences in the predicted fuel-to-air ratios at the wall are less than 5% of their local values, which is an exceptionally good agreement. To a large extent these differences are due to the prescribed shock shape for VSL calculations, which is (even after global iterations) not as good as the implicit shock prediction procedure used in our PNS scheme. These small differences in the predicted C_f values have very little effect on the wall species concentrations. Furthermore, the resulting differences in the wall species concentrations are (probably) within the accuracy of the table-look-up done at the wall to determined these species concentrations.

Figures 4–6 show comparisons of some select species at the body end ($x = 22Rn$). In evaluating these profiles it should be noted that the VSL solutions are for a body-normal coordinate while the PNS predictions are for an axis-normal coordinate. However, the qualitative comparison is certainly valid because the body slope (7 deg) is not very large. The species

concentration profiles of some important carbon-fluorine ablation products, such as CF_4, CF_2, and COF_2, are shown in Fig. 4. The results shows that for these species the profiles are almost identical, with the same peak concentrations and other profile characteristics. There are some differences in the profiles when they decrease to very small numbers (10^{-10} or less), which is probably due to the differences in the two solution schemes. It is important to note the smoothness of the PNS species profiles, which reflects on the accuracy and stability of the PNS solution of the species-conservation equations. Figure 5 shows the species profiles of F_2 and F, and again shows very good agreement between the VSL and PNS predictions. Figure 6 shows a comparison of some of the important ionized species, such as NO^+ and Na^+. Even in this case the VSL and PNS predictions are in very good agreement with each other over most of the significant portion of these species profiles.

The temperature profiles at the body end for this case are shown in Fig. 7. Again the comparison is very good for the major part of the profile. In the outer part of the shock layer, the VSL and PNS predictions of the shock-layer temperature differ by 10–15%. However, on closer inspection, we can see that this difference also exists behind the shock. This indicates that these differences in the outer region are predominantly due to the differences in the bow-shock shape. These preliminary results are very encouraging and show the accuracy of our earlier VSL and present PNS calculations. An important point that is clearly presented by these comparisons is the need to have multiple prediction schemes for such CFD calculations, to provide some means of crosschecking the accuracy of such numerical predictions.

Computing Time Considerations

Apart from the improved solution accuracy provided, the enhanced computing efficiency of the present PNS scheme is another important point. The computing times for case 1 calculations are shown in Table 1. The PNS results shown in this table used 50 axis-normal grid points and 32 points along the body, and took only 30 s on an IBM 3090 (Model 200) machine. This is about three to four times faster than the corresponding VSL solution and is due to the stability, rapid convergence, and computational efficiency of the present PNS scheme.

Case 2 Calculations

The Case 2 PNS solutions were done using two different grids to study the grid-refinement capabilities of our three-dimensional PNS scheme. This test case was also studied using our three-dimensional Teflon-air VSL scheme. In view of the computing times required, these case 2 calculations were only done for a distance of $10Rn$ along the body. The two PNS solutions for this case used 50 and 30 points between the body and the shock, respectively. In each case nine solution planes were used in the circumferential direction. For the 50-points PNS solution the grid spacing at the wall was 0.01% of the local shock-standoff distance, whereas for the 30-point grid this wall spacing was 0.1% of the local shock-standoff distance. The VSL solution for this case used nine circumferential planes and 51 points between the body and the shock. The grid spacing at the wall for this 51-point VSL was 0.05% of the local shock-standoff distance. The following sections deal with some sample results for this test case.

Table 1 Comparison of computing times[a]

Case	Grid[b] $N1\times N2\times N3$	Time, m:s
1	$32\times51\times1$	0:30
2a	$20\times50\times9$	1:50
2b	$21\times30\times9$	1:11

[a]On IBM 3090 (model 200VF) with VS-compiler and scalar OPT = 3 optimization.
[b]$N1$, $N2$, and $N3$ are the number of streamwise, axis-normal, and crossflow grid points.

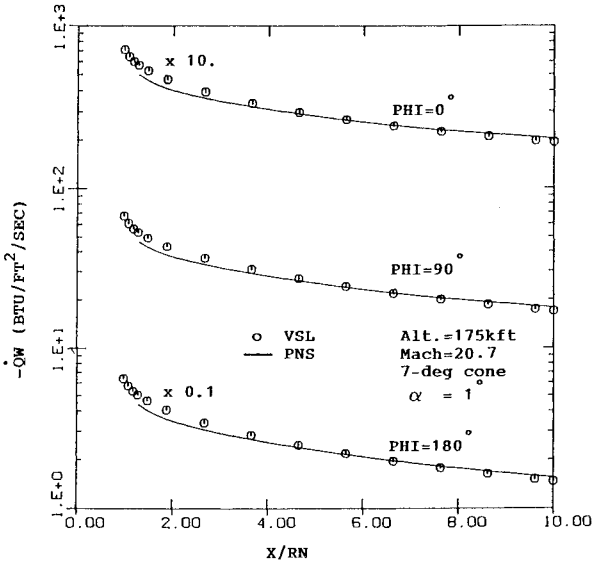

Fig. 8 Axial distribution of wall heat-transfer rates for case 2.

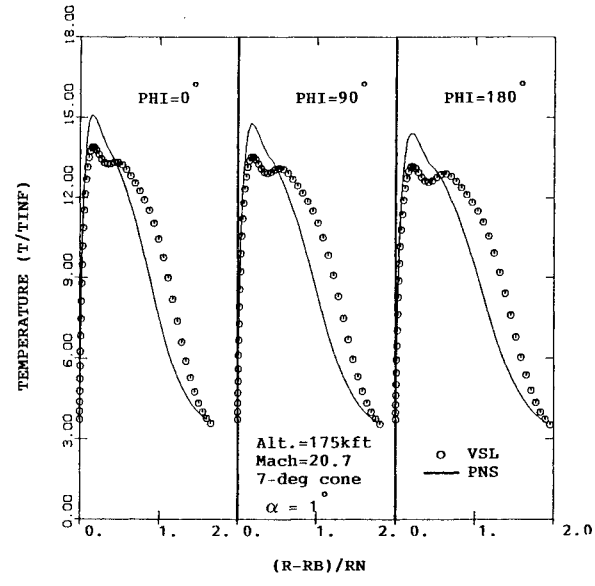

Fig. 9 Temperature profiles at $x/Rn = 10$ for case 2.

Comparison of Surface-Measurable Quantities

The predictions of the total wall heat transfer are compared in Fig. 8. The wall heat transfer shown includes heat transfer due to thermal conduction, heat transfer due to mass diffusion, and heat transfer due to surface ablation. For this case the wall transfer in the afterbody region is conduction dominated. This figure shows that the wall heat-transfer rates predicted by the VSL and PNS schemes are within 5% of each other. Although this agreement is very good, it may be further improved by globally iterating the VSL solution in the afterbody region.

Although not shown here, the results show that the wall-pressure and skin-friction predictions of the VSL and PNS schemes are in very good agreement with each other. The maximum difference in the wall-pressure predictions was approximately 7%, and the maximum difference in the skin-friction predictions was approximately 10%. It should be noted that this VSL solution was not globally iterated. The input inviscid shock used for the VSL calculations differed from the

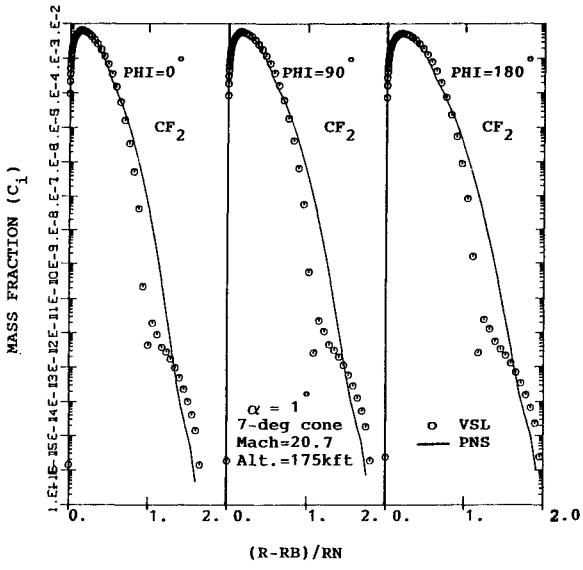

Fig. 10 Concentration profiles of CF_2 at $x/Rn = 10$ for case 2.

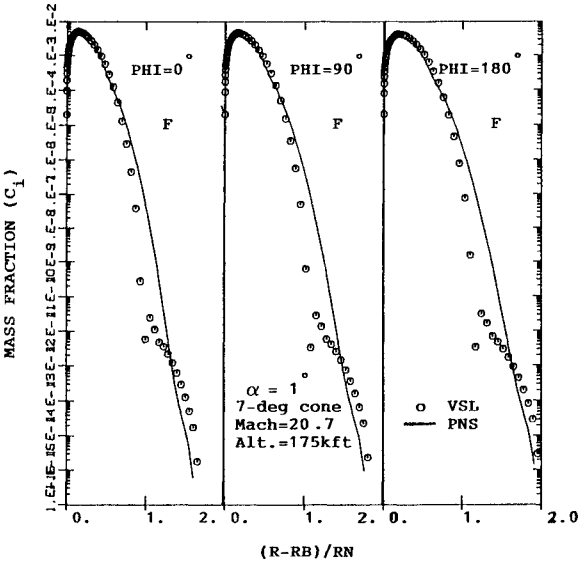

Fig. 11 Concentration profiles of F at $x/Rn = 10$ for case 2.

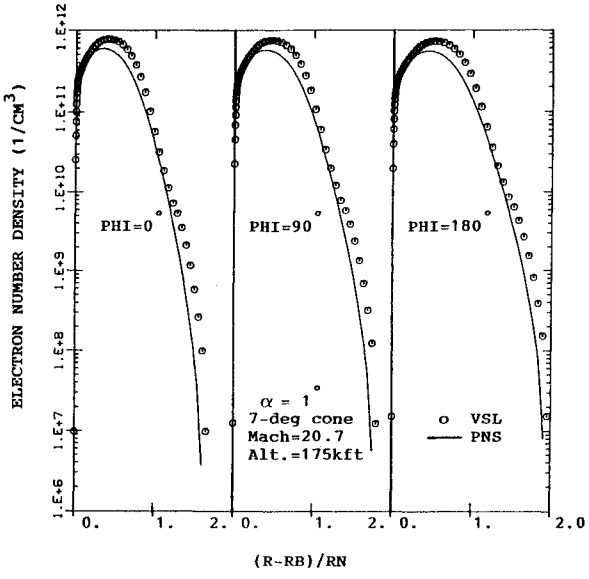

Fig. 12 Electron number density profiles at $x/Rn = 10$ for case 2.

viscous PNS shock by as much as 5%, and this was the primary source of most of the difference in the wall-pressure and skin-friction predictions.

Apart from providing a measure of solution accuracy, these VSL and PNS solutions also show that the three-dimensional Teflon-air VSL scheme provides a very efficient and accurate way of generating the IDP to start the afterbody PNS solution. The accuracy of the nose solution is clearly shown by the smooth match between the VSL and PNS solutions.

Comparison of Species Concentrations

The temperature profiles at the body end are compared in Fig. 9. This figure shows that the peak VSL temperatures are about 10% lower than the corresponding PNS calculations. Furthermore, the VSL results show a small double peak in the temperature profile, whereas the PNS predictions do not show such a behavior. The PNS results do, however, show a small flattening of the temperature profile around the region where the VSL results show the second (smaller) temperature peak. It should be noted that in the VSL results of Fig. 9, the temperature variation around the second (smaller) peak is less than 2% of the local temperature. Differences of such a small magnitude are, however, well within the accuracy of the two numerical solutions being presented.

Figures 10 and 11 show that the peak CF_2 and F_2 concentrations differ by less than 25%. The profiles of electron number density ($1/cm^3$) are shown in Fig. 12, and show that the electron-density peaks predicted by the VSL and PNS codes are within 25% of each other. This peak electron number density is of the order of 10^{11} to 10^{12} electrons/cm^3. Thus, an agreement of within 25% in predicting the electron density is actually very good. Although not shown here, the corresponding VSL and PNS predictions of other species concentrations also agreed very well. For instance, the peak O concentration differed by less than 10%, the minimum O_2 concentration differed by less than 5%, the peak N concentration differed by less than 20%, the minimum N_2 concentration differed by less than 1%, and the peak NO concentrations differed by less than 10%.

Effects of Near-Wall Grid Refinement

To study the effects of body-normal grid refinement on the PNS solution accuracy, we also studied case 2 with a coarser PNS grid between the body and the shock. We used two grids that employed 30 and 50 points between the body and the shock, respectively. In each case the crossflow grid used nine circumferential planes. The predictions of the 30-point grid were in close agreement with the predictions of the 50-point grid, and, thus, are not shown here. Briefly speaking, the wall-pressure predictions differed by less than 1%, and the corresponding differences in the predicted shock-standoff distance were less than 0.5%. The wall heat-transfer and skin-friction predictions differed by less than 10%, and the predictions of the peak electron number density were within 5% of each other.

Computing Time Considerations

The computing times for the various calculations done for this test case are also shown in Table 1. The 30-point PNS solution uses about 1.6 times less grid points that the 50-point PNS solution, and the corresponding computing times are also about 1.6 times less. This is consistent with our general observation that in our three-dimensional PNS scheme the computing times are, typically, linearly proportional to the number of grid points used. In this case the afterbody PNS solution with a 9×50 grid took about one-third the time taken by the corresponding VSL solution using a 9×51 grid.

Conclusions

In this study, a new fully iterative PNS scheme has been developed to study three-dimensional nonequilibrium hypersonic flows over an ablating Teflon surface. Two test cases were considered to study the accuracy and efficiency of this new three-dimensional PNS scheme. These test cases were for 0 and 1 deg angle-of-attack nonequilibrium Teflon-air flows over a sphere-cone vehicle at an altitude of 175 kft and a Mach number of 20. These results substantiate the following conclusions.

1) A new three-dimensional nonequilibrium PNS scheme has been developed for a general curvilinear coordinate system to study the hypersonic flowfields over multiconic configurations with ablating Teflon surfaces. This scheme is inherently stable in the subsonic as well as the supersonic flow regions and does not require the use of any sublayer approximation.

2) A simple yet accurate second-order-accurate smoothing approach has been successfully used to suppress numerical solution oscillations. Furthermore, the axis-normal smoothing effects are limited only to the pressure field, and this results in accurate wall heat-transfer and skin-friction predictions even with coarse axis-normal grids.

3) At the shock a new fully implicit shock-prediction scheme has been developed and used. This scheme uses a general curvilinear coordinate system and predicts the correct shock location without having to make any approximation about the viscous or inviscid nature of the flow behind the shock. Furthermore, this shock-fitting solution is fully coupled in the crossflow direction and results in smooth and accurate shock shapes.

4) A pseudounsteady formulation has been successfully used to solve the governing equations as a sequence of line-by-line block-tridiagonal inversions that converge to the correct result in the limit of convergence. The results show that with this pseudounsteady approach and the ability to take much larger marching steps than noniterative schemes, the present fully iterative three-dimensional results can be obtained accurately and efficiently without any significant computing time penalty.

5) The results of the test cases considered show that the present three-dimensional PNS predictions are in excellent agreement with the corresponding three-dimensional Teflon-air VSL predictions. However, the present PNS calculations take only one-third to one-half the time required for the zeroth global iteration of the corresponding VSL solution. These results clearly demonstrate the accuracy and efficiency of the present three-dimensional Teflon-air PNS scheme.

6) Grid-refinement studies show that the PNS scheme developed has very good grid-refinement characteristics and provides accurate flowfield predictions even when relatively coarse grids are used between the body and the shock.

Acknowledgments

The work reported in this study was supported by the United States Air Force, Headquarters Ballistic Missile Office (BMO/MYES), under Contract F04704-86-C-0031. Captain Tom S. William and Lieutenant Jay Fryer served as the contract monitors on this effort, and Dr. Tony Lin of TRW provided technical guidance. Their cooperation and encouragement during the course of this effort are gratefully acknowledged.

References

[1]Blottner, F. G., Johnson, M., and Ellis, M., "Chemically Reacting Viscous Flow Program for Multi-Component Gas Mixtures," Sandia Laboratories, Albuquerque, NM, Rept. SC-RR-70-754, Dec. 1971.

[2]Swaminathan, S., Kim, M. D., and Lewis, C. H., "Nonequilibrium Viscous Shock-Layer Flows Over Blunt Sphere-Cones at Angles-of-Attack," AIAA Paper 82-0825, June 1982.

[3]Kim, M. D., Swaminathan, S., and Lewis, C. H., "Three-Dimensional Nonequilibrium Viscous Flow Computations Past the Space Shuttle," AIAA Paper 83-0487, Jan. 1983.

[4]Song, D. J., and Lewis, C. H., "Hypersonic Finite-Rate Chemically Reacting Viscous Flows over an Ablating Carbon Surface," *Journal of Spacecraft and Rockets*, Vol. 23, No. 1, 1986, pp. 47-54.

[5]Braun, E. R., "Effects of a Fully Catalytic Wall on a Nonequilibrium Boundary Layer Including Ablating Ablation Products," MS thesis, Polytechnic Institute of Brooklyn, NY, June 1970.

[6]Cresswell, J., Kaplan, B., Porter, R., and Sarcos, C., "Material Effects of Low Temperature Ablators on Hypersonic Wake Properties of Slender Bodies," General Electric Co., Valley Forge, PA, Rept. TIS 67SD255, May 1967.

[7]Finson, M., and Ameer, P., "Non-Equilibrium Boundary-Layer Code," Physical Sciences Inc., Andover, MA, PSI-069/TR-512, May 1985.

[8]Browne, W. G., and Miller, J., "Thermodynamic Properties of Some Ablation Products From Teflon Heat Shields in Air," General Electric Co., Philadelphia, PA, 65SD5315, 1965.

[9]Langan, W. T., Cresswell, J. D., and Browne, W. G., "Effects of Ablation Products on Ionization in Hypersonic Wakes," General Electric Co., Valley Forge, PA, TIS 65SD208, Jan. 1965.

[10]Appleton, J. P., Steinberg, M., and Liquornik, D. J., "Shock-Tube Study of Carbon Monoxide Dissociation Using Vacuum-Ultraviolet Absorption," *Journal of Chemical Physics*, Vol. 52, March 1970, pp. 2205-2221.

[11]Miner, E. W., and Lewis, C. H., "Hypersonic Ionizing Air Viscous Shock-Layer Flows Over Nonanalytic Blunt Bodies," NASA CR-2550, May 1975.

[12]Bortner, M. H., "Chemical Kinetics in a Re-entry Flow Field," General Electric Co., Valley Forge, PA, TIS R63SD63, Aug. 1963.

[13]Schofield, K., "Evaluated Chemical Kinetic Rate Constants for Various Gas Phase Reactions," *Journal of Physical Chemistry Reference Data*, Vol. 2, 1973, pp. 25-84.

[14]Modica, A. P., and LaGraff, J. E., "Thermal Decomposition of C_2F_4 Behind Shock Waves, I. Kinetics and Equilibria of C_2F_4-CF_2 Reaction," AVCO Corp., Wilmington, MA, AVCO RAD-TM-65-3, 1965.

[15]Modica, A. P., and LaGraff, J. E., "Shock Tube Kinetic Studies of the Tetrafluoroethylene-Oxygen System," AVCO Corp., Wilmington, MA, AVCO RAD-TM-65-29, 1965.

[16]Browne, W. G., "Thermodynamic Properties of Some Atoms and Atomic Ions," General Electrical Co., Philadelphia, PA, MSD Engineering Physics TM2, 1962.

[17]Browne, W. G., "Thermodynamic Properties of Some Diatomic and Linear Polyatomic Molecules," General Electrical Co., Philadelphia, PA, MSD Engineering Physics TM3, 1962.

[18]Browne, W. G., "Thermodynamic Properties of Some Diatomic and Diatomic Ions at High Temperatures," General Electric Co., Philadelphia, PA, MSD Engineering Physics TM8, 1962.

[19]Esch, D. D., Siripong, A., and Pike, R. W., "A Technical Report on Thermodynamic Properties in Polynomial Form for Carbon, Hydrogen, Nitrogen, and Oxygen Systems from 300 to 1500 K," NASA-RFL-TR-70-3, Nov. 1970.

[20]Gordon, S., and McBride, B. J., "Computer Program for Calculation of Complex Chemical Equilibrium Compositions, Rocket Performance, Incident, and Reflected Shocks, and Chapman-Jouguet Detonations," NASA SP-273, March 1976.

[21]Browne, W. G., Private Communication, Jan. 1986.

[22]Yos, J. M., "Revised Transport Properties for High Temperature Air and Its Components," Space Systems Division, AVCO Corp., Wilmington, MA, Technical Release, Nov. 28, 1967.

[23]Moss, J. N., "Solutions for Reacting and Nonreacting Viscous Shock Layers with Multicomponent Diffusion and Mass Injection," Ph.D. Dissertation, Virginia Polytechnic Inst. and State Univ., Blacksburg, VA, Oct. 1971.

[24]Moss, J. N., Private Communication, 1984.

[25]Svehla, R. A., "Estimated Viscosities and Thermal Conductivities of Gases at High Temperature," NASA TR-132, 1962.

[26]Neufeld, P. D., Janzen, A. R., and Aziz, R. A., "Empirical Equations to Calculate 16 of the Transport Collision Integrals $\Omega^{(l,s)*}$ for the Lennard-Jones (12-6) potentials," *Journal of Chemical Physics*, Vol. 57, 1972, pp. 1100-1102.

[27]Reid, R. C., Prausnitz, J. M., and Sherwood, T. K., *The Properties of Gases and Liquids*, McGraw-Hill, New York, 1977.

[28]Biolsi, L., Private Communication, Jan. 1986.

[29]Bird, R. B., Stewart, W. E., and Lightfoot, E. N., *Transport Phenomena*, Wiley, New York, NY, 1960, pp. 554-572.

[30]Peyert, R., and Viviand, H., "Computations of Viscous Compressible Flows Based on the Navier-Stokes Equations," AGARD-AG-212, 1975.

[31]Bhutta, B. A., Lewis, C. H., and Kautz, F. A., II, "A Fast Fully-Iterative Parabolized Navier-Stokes Scheme for Chemically-Reacting Reentry Flows," AIAA Paper 85-0926, June 1985.

[32]Bhutta, B. A., and Lewis, C. H., "Low Reynolds Number Flows Past Complex Multiconic Geometries," AIAA Paper 85-0362, Jan. 1985.

[33]Bhutta, B. A., and Lewis, C. H., "An Implicit Parabolized Navier-Stokes Scheme for High-Altitude Reentry Flows," AIAA Paper 85-0036, Jan. 1985.

[34]Bhutta, B. A., and Lewis, C. H., "Prediction and Three-Dimensional Hypersonic Reentry Flows Using a PNS Scheme," *Journal of Spacecraft and Rockets*, Vol. 26, No. 1, 1989, pp. 4–13; also AIAA Paper 85-1604, July 1985.

[35]Bhutta, B. A., and Lewis, C. H., "Parabolized Navier-Stokes Predictions of High-Altitude Reentry Flowfields," VRA, Inc., Blacksburg, VA, VRA-TR-85-02, April 1985.

[36] Schiff, L. B., and Steger, J. L., "Numerical Simulation of Steady Supersonic Viscous Flows," AIAA Paper 79-0130, Jan. 1979.

[37]Kaul, U. K., and Chaussee, D. S., "AFWAL Parabolized Navier-Stokes Code: 1983 AFWAL/NASA Merged Baseline Version," Flight Dynamics Laboratory, Air Force Wright Aeronautical Lab., Wright-Patterson AFB, OH, AFWAL-TR-83-3118, Oct. 1983.

[38]Shanks, S. P., Srinivasan, G. R., and Nicolet, W. E., "AFWAL Parabolized Navier-Stokes Code: Formulation and User's Manual," Air Force Flight Dynamics Lab., Wright Patterson AFB, OH, AFWAL-TR-823034, June 1979.

[39]Helliwell, W. S., Dickinson, R. P., and Lubard, S. C., "Viscous Flows Over Arbitrary Geometries at High Angle of Attack," AIAA Paper 80-0064, Jan. 1980.

[40]Agarwal, R., and Rakich, J. V., "Computation of Hypersonic Laminar Viscous Flow Past Spinning Sharp and Blunt Cones at High Angle of Attack," AIAA Paper 78-0065, Jan. 1978.

[41]Agarwal, R., and Rakich, J. V., "Computation of Supersonic Laminar Viscous Flow Past a Pointed Cone at Angle of Attack in Spinning and Coning Motion," AIAA Paper 78-1211, July 1978.

[42]Pluntze, S. C., "On the Parabolized Navier-Stokes Equations Without Sublayer Approximations," M.Sc. Thesis, Massachusetts Institute of Technology, Cambridge, MA, Jan. 1987.

[43]Baron, J. R., Private Communication, 1987.

[44]Thompson, R. A., Lewis, C. H., and Kautz, F. A., II, "Comparison Techniques for Predicting 3-D Viscous Flows Over Ablated Shapes," AIAA Paper 83-0345, Jan. 1983.

[45]Baron, J. R., "The Binary Boundary Layer Associated with Mass Transfer at High Speeds," Massachusetts Institute of Technology, Naval Supersonic Lab., Cambridge, MA, TR160, 1956.

[46]Chaussee, D. S., Patterson, J. L., Kutler, P., Pulliam, T. H., and Steger, J. L., "A Numerical Simulation for Hypersonic Viscous Flows Over Arbitrary Geometries at High Angle of Attack," AIAA Paper 81-0050, Jan. 1981.

[47]Lubard, S. C., and Helliwell, W. S., "Calculation of the Flow on a Cone at High Angle of Attack," R&D Associates, Santa Monica, CA, Rept. RDA-TR-150, Feb. 1973.

[48]Bhutta, B. A., and Lewis, C. H., "Three-Dimensional Parabolized Navier-Stokes Predictions of Hypersonic Nonequilibrium Flows over Ablating Teflon Surfaces, Vols. 1 and 2," VRA, Inc., Blacksburg, VA, VRA-TR-87-02, Dec. 1987.

Walter B. Sturek
Associate Editor